# Prediction of double-Weyl points in the iron-based superconductor math xmlns="http://www.w3.org/1998/Math/MathML">mrow>mi>Ca/mi>mi mathvariant="normal">K/mi>msub>mi>Fe/mi>mn>4/mn>/msub>msub>mi>As/mi>mn>4/mn>/msub>/mrow>/math>

Niclas Heinsdorf, Morten H. Christensen, Mikel Iraola, Shang-Shun Zhang, Fan Yang, Turan Birol, Cristian D. Batista, Roser Valentí, and Rafael M. Fernandes

# Prediction of Double-Weyl Points in the Iron-Based Superconductor $CaKFe_4As_4$

Niclas Heinsdorf,[1, *] Morten H. Christensen,[2, †] Mikel Iraola,[1, 3, 4] Shang-Shun Zhang,[5] Fan Yang,[6] Turan Birol,[6] Cristian D. Batista,[5, 7, ‡] Roser Valentí,[1, §] and Rafael M. Fernandes[2, ¶]

[1]*Institut für Theoretische Physik, Goethe-Universität Frankfurt, Max-von-Laue-Strasse 1, 60438 Frankfurt am Main, Germany*
[2]*School of Physics and Astronomy, University of Minnesota, Minneapolis, 55455 MN*
[3]*Department of Condensed Matter Physics, University of the Basque Country UPV/EHU, Apartado 644, 48080 Bilbao, Spain*
[4]*Donostia International Physics Center, 20018 Donostia-San Sebastian, Spain*
[5]*Department of Physics and Astronomy, The University of Tennessee, Knoxville, Tennessee 37996, USA*
[6]*Department of Chemical Engineering and Materials Science, University of Minnesota, Minneapolis, 55455 MN*
[7]*Neutron Scattering Division and Shull-Wollan Center, Oak Ridge National Laboratory, Oak Ridge, Tennessee 37831, USA*
(Dated: July 13, 2021)

Employing a combination of symmetry analysis, low-energy modeling, and *ab initio* simulations, we predict the presence of magnetic-field-induced Weyl points close to the Fermi level in $CaKFe_4As_4$. Depending on the relative strengths of the magnetic field and of the spin-orbit coupling, the Weyl fermions can carry a topological charge of $\pm 1$ or $\pm 2$, making $CaKFe_4As_4$ a rare realization of a double-Weyl semimetal. We further predict experimental manifestations of these Weyl points, both in bulk properties, such as the anomalous Hall effect, and in surface properties, such as the emergence of prominent Fermi arcs. Because $CaKFe_4As_4$ displays unconventional fully-gapped superconductivity below 30 K, our findings open a novel route to investigate the interplay between superconductivity and Weyl fermions.

The realization of topological phenomena in iron-based superconductors has opened a new route to elucidate the interplay between topology, electronic correlations, and unconventional superconductivity. Indeed, a band inversion involving an As/Se $p_z$-band and a pair of Fe $d_{xz}/d_{yz}$-bands along the $\Gamma$-$Z$ line of the Brillouin zone has been observed in several compounds, such as $FeTe_{1-x}Se_x$, $LiFe_{1-x}Co_xAs$, and $CaKFe_4As_4$ [1–6]. In the normal state, such a band inversion gives rise to helical Dirac states at the surface and semimetallic Dirac states in the bulk. In the superconducting state, zero-energy states are observed inside some (but not all) vortices, suggesting the presence of Majorana bound states [7–11], whereas a flat density of states is seen at domain walls, characteristic of linearly-dispersing one-dimensional Majorana modes [12].

In this paper, we show that another non-trivial topological phenomenon – Weyl points – can be realized in the iron-based superconductor $CaKFe_4As_4$ in a magnetic field. The existence of these Weyl fermions, which are anchored in a fourfold rotational symmetry of the lattice, does not rely on a $p$-$d$ band inversion, but on the fact that each Fe plane in this bilayer compound lacks inversion symmetry. Unlike the other iron-based superconductors, the inversion centers of $CaKFe_4As_4$ are not on the Fe layer, but at the positions of the Ca and K atoms. Consequently, there is no glide-plane symmetry either. While the inversion symmetries on the Fe layers are broken explicitly by the lattice, the effect is enhanced by magnetic fluctuations associated with the nearby spin-vortex crystal state realized in weakly electron-doped $CaKFe_4As_4$ [13].

Our combined analysis involving symmetry considerations and *ab initio* simulations demonstrates that, in the presence of a magnetic field, a pair of Weyl points emerge close to the Fermi energy along the high-symmetry $M$-$A$ [i.e. $(\pi, \pi, 0)$-$(\pi, \pi, \pi)$] line of the Brillouin zone. Whereas a number of inversion-symmetry-broken Weyl semimetals have been reported [14–26], time-reversal symmetry-broken Weyl semimetals seem more scarce [27–36]. Importantly, in $CaKFe_4As_4$ we show that depending on the relative magnitudes of the splittings of energy levels at the $M$ point caused by the Zeeman field, by the bilayer coupling, and by the spin-orbit coupling, Weyl points can arise from crossings between bands of opposite or equal spin polarization. In the latter case, which we explicitly verify in our *ab initio* calculations, the Weyl fermions carry a higher order topological charge of $\pm 2$, making $CaKFe_4As_4$ a *double*-Weyl semimetal. Experimentally, we propose that the presence of Weyl fermions can be probed by transport measurements of the anomalous Hall effect and by spectroscopic detection of the characteristic Fermi arcs that we obtain in our analysis.

We propose that the separation between the Weyl points and the Fermi level is reduced not only by hole doping, but also by electronic correlations, which are known to generally shrink the bands in iron-based superconductors [37–42]. Moreover, since the orbitals from which the Weyl points originate are the same $d$-orbitals that become superconducting below $T_c \approx 30$ K, $CaKFe_4As_4$ provides a promising framework to realize an intrinsic unconventional superconducting double-Weyl semimetal.

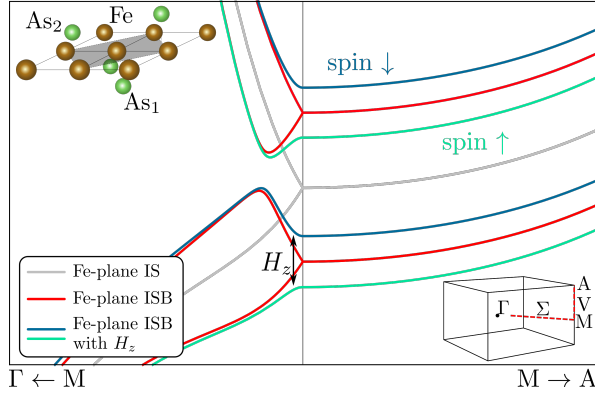We first consider a single FeAs layer with $P4/nmm$

FIG. 1. Schematic of the symmetries and band-dispersion degeneracies of a single FeAs layer with $P4/nmm$ space group. Including spin-orbit coupling, the glide-plane symmetry enforces fourfold degenerate bands along the $M$-$A$ line and twofold degenerate bands along $\Gamma$-$M$ (gray curves). Breaking of the Fe-plane inversion symmetry (IS) by making the two As atoms above and below the plane inequivalent (upper inset) lowers the degeneracies of the bands to twofold along $M$-$A$ and one-fold along $\Gamma$-$M$ (red curves). Application of a perpendicular magnetic field ($H_z$) in the Fe-plane inversion-symmetry broken (ISB) case makes all bands non-degenerate (green and blue curves). The lower inset shows the Brillouin zone, with $\Gamma = (0,0,0)$, $M = (\pi, \pi, 0)$ and $A = (\pi, \pi, \pi)$.

(#129) space group, and analyze which symmetries need to be broken in order to obtain non-degenerate bands, whose crossings can result in Weyl points. The system has an inversion center on the Fe plane and, due to the puckering of the As atoms above and below the Fe plane, a glide-plane symmetry consisting of a reflection with respect to the Fe plane followed by a half unit-cell translation along the in-plane diagonal (upper inset of Fig. 1). The combination of this Fe-plane centered inversion symmetry with time-reversal symmetry leads to a Kramers degeneracy of the bands over the whole Brillouin zone, as illustrated in Fig. 1 by the twofold degenerate bands along the in-plane $\Gamma$-$M$ direction. The energy states at the $M$ point, however, are fourfold degenerate, even in the presence of spin-orbit coupling (SOC), due to the glide-plane symmetry of the space group [43, 44] (gray curves in Fig. 1).

For a simple stacking of FeAs layers (i.e. a stacking that preserves the non-symmorphic $P4/nmm$ space group of a single layer, like in FeSe or LiFeAs), the band degeneracies at the $M$ point extend along the entire $M$-$A$ line. When inversion symmetry centered on the Fe plane is broken so that the space group is reduced to $P4mm$, either explicitly by a substrate [45] or spontaneously by interactions that favor a spin-vortex crystal magnetic ground state [13], the glide-plane symmetry is also broken and some of these degeneracies are lifted. As shown by the red curves in Fig. 1, the fourfold degenerate bands along $M$-$A$ split into pairs of twofold degenerate

bands in the presence of SOC. Along the in-plane $\Gamma$-$M$ line, all bands become non-degenerate, as previously discussed in Ref. [46]. The remaining twofold degeneracy of the energy levels along $M$-$A$ can be lifted by the Zeeman coupling to an external out-of-plane magnetic field, as shown by the green and blue curves in Fig. 1. Depending on the band structure parameters and on the magnitude of the magnetic field, these non-degenerate bands can potentially cross, yielding a pair of Weyl points at $(\pi, \pi, \pm k_z)$.

Having established a general framework in which Weyl points can potentially arise in iron-based superconductors, we now turn our attention to a specific material. An ideal candidate to realize this effect is the bilayer $CaKFe_4As_4$, since the individual FeAs layers lack inversion symmetry [see Fig. 3(a)]. Indeed, this material crystallizes in the symmorphic tetragonal space group $P4/mmm$ (#123) with lattice constants $a = b = 3.8659$ Å and $c = 12.884$ Å. The fourfold rotational symmetry about the $z$-axis, $C_4^z$, is centered at either the middle of the conventional unit cell or at one of its four corners. The distinguishing feature of this crystalline structure is that the alternating layers of Ca and K make the two As atoms inequivalent, thus breaking the glide plane symmetry present in all other iron-based superconductors. This results in a polar structure for the Fe layers, since the site-symmetry of the Fe atoms is $2mm$ ($C_{2v}$), with no mirror plane or center of inversion on the Fe layer. Moreover, because $CaKFe_4As_4$ is at the verge of spin-vortex crystal order [13], magnetic fluctuations are expected to enhance the impact of the explicit glide-plane symmetry-breaking on the low-energy electronic states.

In contrast to the single-layer case discussed in the context of Fig. 1, the unit cell of $CaKFe_4As_4$ contains two Fe layers. This ensures the existence of an inversion center on the Ca and K sites, which in turn preserves the Kramers degeneracy of the bands for every momentum. To verify whether Weyl points can still emerge for this bilayer stacking configuration, we first perform a group-theoretical analysis appropriate for the space group $P4/mmm$, focusing on the $\Gamma$-$M$-$A$ path.

We consider first the case without magnetic field or SOC, where all bands are spin-degenerate. As shown schematically in Fig. 2(a), which is based on our density functional theory (DFT) calculations, the band structure along the $\Gamma$-$M$ line consists of four bands that transform as the single-valued representations $\Sigma_{1-4}$ [47, 48]. Due to the $C_4^z$ symmetry at $M$, these bands become pairwise degenerate at $M$, transforming under the two-dimensional irreducible representations (irreps) $M_5^\pm$. Microscopically, the energy splitting between the $M_5^\pm$ energy levels is set by the strength of the coupling between the two FeAs layers. Both the $M_5^+$ and the $M_5^-$ irreps have basis functions with $C_4^z$ eigenvalues $\mp i$, which are related to the orbital moments of the wave-functions. Because the $C_4^z$ axis does not cross the Fe atoms, the or-
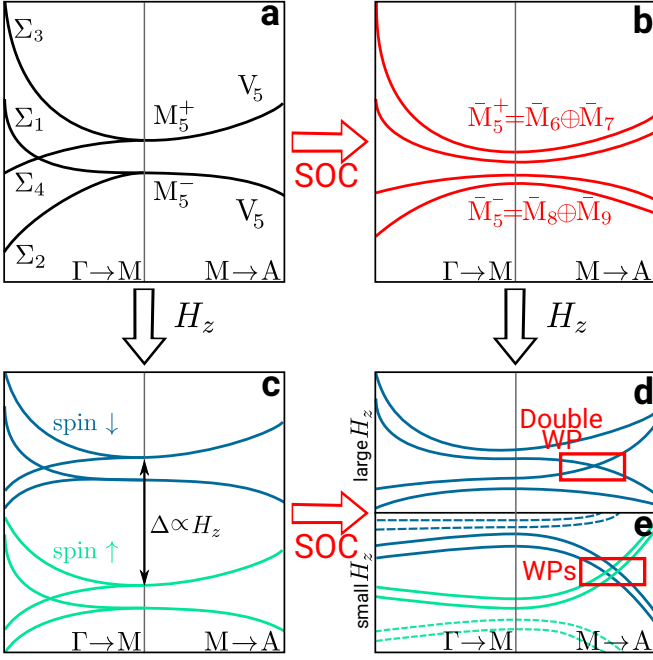
FIG. 2. (a) Schematic band structure of CaKFe$_4$As$_4$ along $\Gamma$-$M$ and $M$-$A$. Four bands, transforming under the irreps $\Sigma_{1-4}$, become pairwise degenerate at $M$, where they transform as $M_5^{\pm}$. Along $M$-$A$, they form nodal lines (transforming as $V_5$) which, due to Kramers degeneracy, are fourfold degenerate. (b) In the presence of SOC, the bands transform as the double-valued reducible representations $\bar{M}_5^{\pm}$. The two nodal lines are split into four bands that remain Kramers degenerate. (c) In the presence of a magnetic field (but no SOC), the Kramers degeneracy is split into a spin-$\uparrow$ and a spin-$\downarrow$ branch. The Zeeman splitting $\Delta$ is proportional to the field $H_z$. (d)-(e) In the presence of both SOC and a magnetic field, the bands become non-degenerate, and an accidental intersection can occur, resulting in a Weyl point (WP). Its topological charge $\mathcal{C}$ depends on whether the crossing involves bands of the same spin ($\mathcal{C} = \pm 2$, resulting in a double WP, panel (d)) or opposite spins ($\mathcal{C} = \pm 1$, resulting in a single WP, panel (e)).

bital moments are not those of the individual Fe atomic orbitals. Instead, they are determined by the relative phase of the wave-functions on the two different Fe sites on the same plane in the unit cell, which is related to the orbital angular momentum on a four iron molecular orbital. Continuing along the $M$-$A$ line in Fig. 2(a), the bands remain pairwise degenerate, transforming as $V_5$. The total degeneracy of each of these bands is four, due to the Kramers degeneracy enforced by the composition of inversion and time-reversal symmetries.

There are two different ways to break this fourfold degeneracy. One is to turn on the SOC, as shown in Fig. 2(b). In this case, we must consider the symmetries of the double-valued space group, which explicitly accounts for the spin-1/2 of the electrons. Because at the $M$ point the double group has no four-dimensional rep-

resentations, the two fourfold degenerate bands split in four twofold degenerate bands. This remaining twofold degeneracy is a consequence of the fact that the Kramers degeneracy is preserved by SOC.

The bands at $M$ transform as the two-dimensional pseudo-real irreps $\bar{M}_6$, $\bar{M}_7$, $\bar{M}_8$, and $\bar{M}_9$ of the double-group, whose $C_4^z$ eigenvalues are either $e^{\mp i 3\pi/4}$ (for $\bar{M}_{6,8}$) or $e^{\mp i\pi/4}$ (for $\bar{M}_{7,9}$) [48]. The extra factor of $e^{\mp i\pi/4}$ with respect to the original $C_4^z$ eigenvalues of $M_5^{\pm}$ originates from the spin angular momentum, such that the eigenvalues in the double-group correspond to the $z$ component of the total angular momentum ($\mathbf{L} + \mathbf{S}$) of the electron.

An alternative way to break the fourfold degeneracy of the $M$-$A$ bands in Fig. 2(a) is to break time-reversal symmetry by applying an external magnetic field parallel to the $z$-axis, as indicated in Fig. 2(c). In this case, each band is split into two spin branches, denoted by spin-$\uparrow$ and spin-$\downarrow$. Their energy splitting $\Delta$ is proportional to the magnetic field $H_z$. The reason why the $M$-$A$ bands retain a twofold degeneracy, even though the Kramers degeneracy is absent, is because of the non-Abelian nature of the little group on the $M$-$A$ line, which is isomorphic to the magnetic space group $P42'2'$ (#89.90).

Combining both SOC and $H_z$, all bands become non-degenerate. Depending on the values of the bilayer splitting between $M_5^{\pm}$ [Fig. 2(a)], the SOC splitting between $\bar{M}_{6,7}$ [Fig. 2(b)], and the Zeeman splitting $\Delta$ between the spin-$\uparrow$ and spin-$\downarrow$ branches [Fig. 2(c)], crossings of these non-degenerate bands may occur along the $M$-$A$ line, resulting in the Weyl points shown in Figs. 2(d)-(e). Of course, among these three parameters, the only one that can be efficiently tuned experimentally is $\Delta$. Although group theory cannot predict the existence and positions of these crossings, it can be employed to identify two different scenarios. When $\Delta$ is large compared to the SOC and bilayer splittings, crossings between states with the *same spin orientation* and opposite orbital angular momentum can occur, as shown in Fig. 2(d). Because, as explained above, states of opposite orbital angular momentum have $C_4^z$ eigenvalues $\pm i$, their ratio is equal to $-1$, resulting in double-Weyl points with topological charge $\mathcal{C} = \pm 2$ [49]. On the other hand, when $\Delta$ is small compared to the SOC and bilayer splittings, the crossing can involve states with *opposite spin states* but the same orbital angular momentum, as illustrated in Fig. 2(e). In this case, the ratio between the $C_4^z$ eigenvalues of the crossing bands is equal to $\pm i$, yielding a single-Weyl point with $\mathcal{C} = \pm 1$. In either scenario, note that the Weyl points are anchored in the $C_4^z$ symmetry of the crystal.

To verify whether Weyl points emerge in CaKFe$_4$As$_4$, in Fig. 3(c) we present relativistic DFT calculations of the electronic band structure obtained with the Full Potential Local Orbital (FPLO) code [50] within the generalized gradient approximation (GGA) [51]. To model the effects of an external magnetic field, we assume a
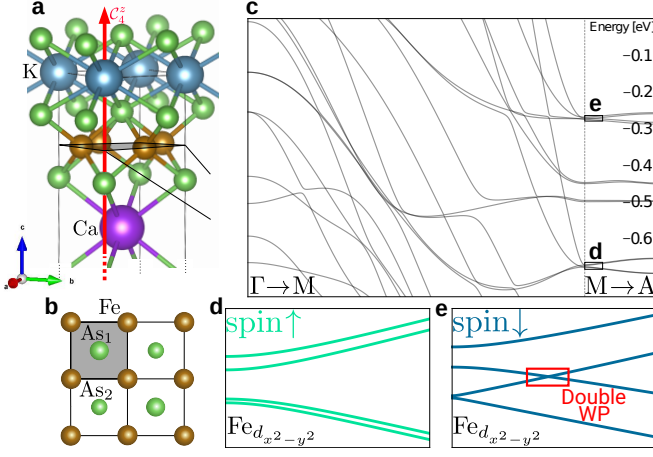
FIG. 3. (a) Upper half of the crystal structure of CaKFe$_4$As$_4$ and (b) top view of four iron plaquettes. (c) DFT band structure in the presence of finite Fe magnetization and SOC calculated with the FPLO basis [50]. A double Weyl-point involving Fe $d_{x^2-y^2}$ orbitals with equal spin emerges. (d) and (e) are zooms of the regions denoted in (c), indicating where the double Weyl point appears.

ferromagnetic configuration for the Fe atoms, converging the structure self-consistently with a fixed total magnetic moment. We initiate the calculations with magnetic moments pointing along the [001] direction, resulting in an out-of-plane magnetic moment of $\mu_{\text{Fe}} = 0.63\mu_B$ on the Fe atoms and $\mu_{\text{As}} = -0.13\mu_B$ on the As atoms. Fig. 3(e) shows a crossing between two $d_{x^2-y^2}$ bands in the spin-$\downarrow$ branch. We thus identify a pair of Weyl points located at $\mathbf{k}_0^\pm = (1/2, 1/2, \pm 0.0178)2\pi/a$ and 0.27eV below the Fermi level. On the other hand, the spin-$\uparrow$ branch in Fig. 3(d), which is pushed down in energy by the Zeeman splitting, does not exhibit any band crossing. We note that due to the distinct locations of the spin-$\uparrow$ and -$\downarrow$ branches in the energy spectrum, the bands hybridize differently with surrounding As $4p$-bands. Decreasing the magnetization of the Fe atoms first reveals a tendency of the Weyl points to annihilate as they move towards the M point. Upon further suppression of the moment, we observe band crossings consistent with single Weyl points as depicted in Fig. 2(e) (see the SM [48] for more details).

As expected from the above symmetry analysis, by expanding the band dispersion in the vicinity of the two Weyl points at $\mathbf{k}_0^\pm$, we find that they disperse linearly along the $k_z$ direction but quadratically in the $(k_x, k_y)$-plane (see Fig. 4(c)). Thus, the corresponding $\mathbf{k} \cdot \mathbf{p}$ Hamiltonian [52] is:

$$\mathcal{H} = m\sigma_z + (ak_+^2 + bk_-^2)\sigma_+ + h.c., \tag{1}$$

with $k_\pm = k_x \pm ik_y$ and Pauli matrices $\sigma_i$ defined in the subspace of the two bands. As a result, a double Weyl point with topological charge $\mathcal{C} = \pm 2$ is realized. This is verified by directly computing the Berry curvature flux
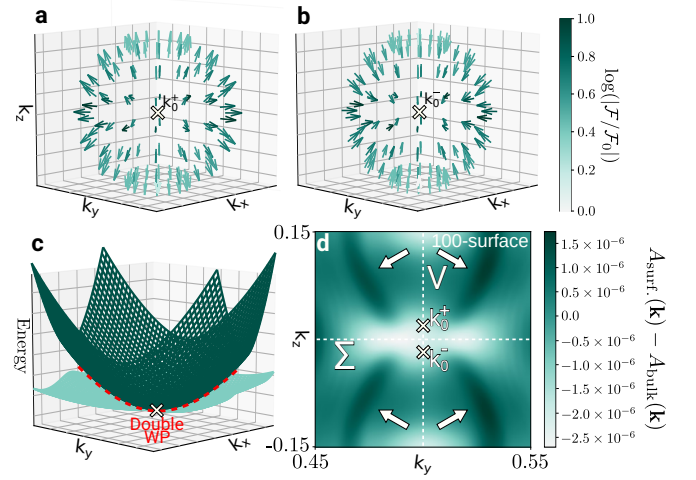


FIG. 4. Berry curvature flux $\mathcal{F}$ on momentum-space spheres of radius $0.002\pi/a$ centered at (a) $\mathbf{k}_0^+$ and (b) $\mathbf{k}_0^-$. The vectors have been normalized and their magnitudes are indicated by their color. Upon integration of $\mathcal{F}$, we obtain the topological charges $\mathcal{C} = \pm 2$ characteristic of double-Weyl points. (c) Energy dispersion of the two bands forming the Weyl point near $\mathbf{k}_0^+$. Although they intersect linearly along $k_z$, a quadratic touching is realized in the $(k_x, k_y)$-plane. (d) Spectral density $A(\mathbf{k})$ calculated from DFT across the (100) surface. The Fermi arcs are indicated by white arrows. In order to enhance the contrast, we performed semi-slab and bulk calculations and subtracted the latter from the former.

across two small spheres enclosing the Weyl points from our DFT calculations. As shown in Figs. 4(a)-(b), the two nodes act as a source and a sink of Berry flux $\mathcal{F}$, represented by the vector field. Integrating the Berry flux numerically, we indeed obtain topological charges $\mathcal{C} = \pm 2$. This non-trivial topological charge is expected to manifest itself experimentally as an anomalous Hall effect (AHE) [53, 54]. Another typical manifestation of Weyl fermions is the emergence of Fermi arcs on the sample's surfaces. In Fig. 4(d), we show the $k$-resolved spectral density on the (100) surface at the energy where the Weyl points are located. Two pronounced Fermi arcs are identified, as indicated by the white arrows, terminating at the two Weyl points, denoted by the crosses.

To experimentally observe these manifestations of the Weyl fermions – AHE and Fermi arcs – it is desirable that the Weyl points are close to the Fermi level $E_F$. In our DFT calculations, they are located 0.27 eV below $E_F$. However, it is well-established that DFT overestimates the energies of the bottom/top of the bands, which are reduced by correlations [37–42]. Previous comparison between DFT results and ARPES measurements on CaKFe$_4$As$_4$ in the absence of a magnetic field [55] suggests that the bottom of the electron pocket at the M point shifts upwards by a factor of 5 in the actual material; such a renormalization would bring the Weyl point to within $\sim 50$ meV of the Fermi level. Moreover, hole

doping could be used to further tune the Fermi energy to the desired position.

In summary, we demonstrated that the breaking of the Fe-plane inversion symmetry in iron-based superconductors, combined with an external magnetic field, provide a promising route to realize Weyl points in these materials. While our focus here was on $CaKFe_4As_4$, the general symmetry arguments are expected to apply to any other iron-based material whose Fe layers lack inversion symmetry. The latter is expected to happen, for instance, in thin films of single-layer compounds [56], since the substrate explicitly breaks the inversion symmetry. Alternatively, it can take place as a spontaneous symmetry-breaking driven by interactions that favor the spin-vortex crystal magnetic ground state, which was recently observed in the phase diagram $Ba_{1-x}Na_xFe_2As_2$ [57].

More broadly, the realization of Weyl points in iron-based materials would open the door to investigate the interplay between Weyl fermions and other types of electronic orders not usually present in the currently studied Weyl semimetals. For instance, spontaneous nematic order or applied uniaxial strain would break the $C_4^z$ symmetry and split the double-Weyl points into two single-Weyl points (see [48] for more details). Another interesting route would be to probe the impact of unconventional superconductivity, which onsets below 30K in $CaKFe_4As_4$, on the Weyl fermions and the associated Fermi arcs.

* heinsdorf@itp.uni-frankfurt.de
† Present Address: Center for Quantum Devices, Niels Bohr Institute, University of Copenhagen, Copenhagen 2100, Denmark
‡ cbatist2@utk.edu
§ valenti@itp.uni-frankfurt.de
¶ rfernand@umn.de

[1] Z. Wang, P. Zhang, G. Xu, L. K. Zeng, H. Miao, X. Xu, T. Qian, H. Weng, P. Richard, A. V. Fedorov, H. Ding, X. Dai, and Z. Fang, Phys. Rev. B **92**, 115119 (2015).

[2] X. Wu, S. Qin, Y. Liang, H. Fan, and J. Hu, Physical Review B **93**, 115129 (2016).

[3] P. Zhang, Z. Wang, X. Wu, K. Yaji, Y. Ishida, Y. Kohama, G. Dai, Y. Sun, C. Bareille, K. Kuroda, *et al.*, Nature Physics **15**, 41 (2019).

[4] H. Lohani, T. Hazra, A. Ribak, Y. Nitzav, H. Fu, B. Yan, M. Randeria, and A. Kanigel, Phys. Rev. B **101**, 245146 (2020).

[5] S. Borisenko, V. Bezguba, A. Fedorov, Y. Kushnirenko, V. Voroshnin, M. Sturza, S. Aswartham, and A. Yaresko, npj Quantum Materials **5**, 67 (2020).

[6] W. Liu, L. Cao, S. Zhu, L. Kong, G. Wang, M. Papaj, P. Zhang, Y.-B. Liu, H. Chen, G. Li, F. Yang, T. Kondo, S. Du, G.-H. Cao, S. Shin, L. Fu, Z. Yin, H.-J. Gao, and H. Ding, Nature Communications **11**, 5688 (2020).

[7] J.-X. Yin, Z. Wu, J.-H. Wang, Z.-Y. Ye, J. Gong, X.-Y. Hou, L. Shan, A. Li, X.-J. Liang, X.-X. Wu, J. Li, C.-S. Ting, Z.-Q. Wang, J.-P. Hu, P.-H. Hor, H. Ding, and S. H. Pan, Nature Physics **11**, 543 (2015).

[8] D. Wang, L. Kong, P. Fan, H. Chen, S. Zhu, W. Liu, L. Cao, Y. Sun, S. Du, J. Schneeloch, *et al.*, Science **362**, 333 (2018).

[9] Q. Liu, C. Chen, T. Zhang, R. Peng, Y.-J. Yan, X. Lou, Y.-L. Huang, J.-P. Tian, X.-L. Dong, G.-W. Wang, *et al.*, Physical Review X **8**, 041056 (2018).

[10] T. Machida, Y. Sun, S. Pyon, S. Takeda, Y. Kohsaka, T. Hanaguri, T. Sasagawa, and T. Tamegai, Nature Materials **18**, 811 (2019).

[11] L. Kong, L. Cao, S. Zhu, M. Papaj, G. Dai, G. Li, P. Fan, W. Liu, F. Yang, X. Wang, S. Du, C. Jin, L. Fu, H.-J. Gao, and H. Ding, "Tunable vortex majorana zero modes in lifeas superconductor," (2020), arXiv:2010.04735 [cond-mat.supr-con].

[12] Z. Wang, J. O. Rodriguez, L. Jiao, S. Howard, M. Graham, G. Gu, T. L. Hughes, D. K. Morr, and V. Madhavan, Science **367**, 104 (2020).

[13] W. R. Meier, Q.-P. Ding, A. Kreyssig, S. L. Bud'ko, A. Sapkota, K. Kothapalli, V. Borisov, R. Valentí, C. D. Batista, P. P. Orth, R. M. Fernandes, A. I. Goldman, Y. Furukawa, A. E. Böhmer, and P. C. Canfield, npj Quantum Materials **3**, 5 (2018).

[14] S.-M. Huang, S.-Y. Xu, I. Belopolski, C.-C. Lee, G. Chang, B. Wang, N. Alidoust, G. Bian, M. Neupane, C. Zhang, *et al.*, Nature communications **6**, 1 (2015).

[15] H. Weng, C. Fang, Z. Fang, B. A. Bernevig, and X. Dai, Physical Review X **5**, 011029 (2015).

[16] N. Xu, H. Weng, B. Lv, C. E. Matt, J. Park, F. Bisti, V. N. Strocov, D. Gawryluk, E. Pomjakushina, K. Conder, *et al.*, Nature communications **7**, 1 (2016).

[17] S.-Y. Xu, I. Belopolski, N. Alidoust, M. Neupane, G. Bian, C. Zhang, R. Sankar, G. Chang, Z. Yuan, C.-C. Lee, *et al.*, Science **349**, 613 (2015).

[18] S.-Y. Xu, N. Alidoust, I. Belopolski, Z. Yuan, G. Bian, T.-R. Chang, H. Zheng, V. N. Strocov, D. S. Sanchez, G. Chang, *et al.*, Nature Physics **11**, 748 (2015).

[19] L. Yang, Z. Liu, Y. Sun, H. Peng, H. Yang, T. Zhang, B. Zhou, Y. Zhang, Y. Guo, M. Rahn, *et al.*, Nature

physics **11**, 728 (2015).

[20] J. Ruan, S.-K. Jian, H. Yao, H. Zhang, S.-C. Zhang, and D. Xing, Nature communications **7**, 1 (2016).

[21] A. A. Soluyanov, D. Gresch, Z. Wang, Q. Wu, M. Troyer, X. Dai, and B. A. Bernevig, Nature **527**, 495 (2015).

[22] Y. Sun, S.-C. Wu, M. N. Ali, C. Felser, and B. Yan, Physical Review B **92**, 161107 (2015).

[23] Z. Wang, D. Gresch, A. A. Soluyanov, W. Xie, S. Kushwaha, X. Dai, M. Troyer, R. J. Cava, and B. A. Bernevig, Physical review letters **117**, 056805 (2016).

[24] T.-R. Chang, S.-Y. Xu, G. Chang, C.-C. Lee, S.-M. Huang, B. Wang, G. Bian, H. Zheng, D. S. Sanchez, I. Belopolski, *et al.*, Nature communications **7**, 1 (2016).

[25] G. Chang, B. Singh, S.-Y. Xu, G. Bian, S.-M. Huang, C.-H. Hsu, I. Belopolski, N. Alidoust, D. S. Sanchez, H. Zheng, *et al.*, Physical Review B **97**, 041104 (2018).

[26] S.-Y. Xu, N. Alidoust, G. Chang, H. Lu, B. Singh, I. Belopolski, D. Sanchez, X. Zhang, G. Bian, H. Zheng, *et al.*, arXiv preprint arXiv:1603.07318 (2016).

[27] X. Wan, A. M. Turner, A. Vishwanath, and S. Y. Savrasov, Physical Review B **83**, 205101 (2011).

[28] S. Borisenko, D. Evtushinsky, Q. Gibson, A. Yaresko, T. Kim, M. Ali, B. Buechner, M. Hoesch, and R. J. Cava, arXiv preprint arXiv:1507.04847 (2015).

[29] M. Chinotti, A. Pal, W. Ren, C. Petrovic, and L. Degiorgi, Physical Review B **94**, 245101 (2016).

[30] G. Chang, S.-Y. Xu, H. Zheng, B. Singh, C.-H. Hsu, G. Bian, N. Alidoust, I. Belopolski, D. S. Sanchez, S. Zhang, *et al.*, Scientific reports **6**, 1 (2016).

[31] Z. Wang, M. Vergniory, S. Kushwaha, M. Hirschberger, E. Chulkov, A. Ernst, N. P. Ong, R. J. Cava, and B. A. Bernevig, Physical review letters **117**, 236401 (2016).

[32] M. Hirschberger, S. Kushwaha, Z. Wang, Q. Gibson, S. Liang, C. A. Belvin, B. A. Bernevig, R. J. Cava, and N. P. Ong, Nature materials **15**, 1161 (2016).

[33] C. Shekhar, A. K. Nayak, S. Singh, N. Kumar, S.-C. Wu, Y. Zhang, A. C. Komarek, E. Kampert, Y. Skourski, J. Wosnitza, *et al.*, arXiv preprint arXiv:1604.01641 (2016).

[34] T. Suzuki, R. Chisnell, A. Devarakonda, Y.-T. Liu, W. Feng, D. Xiao, J. W. Lynn, and J. Checkelsky, Nature Physics **12**, 1119 (2016).

[35] H. Yang, Y. Sun, Y. Zhang, W.-J. Shi, S. S. Parkin, and B. Yan, New Journal of Physics **19**, 015008 (2017).

[36] Y. Zhang, Y. Sun, H. Yang, J. Železnỳ, S. P. Parkin, C. Felser, and B. Yan, Physical Review B **95**, 075128 (2017).

[37] L. Ortenzi, E. Cappelluti, L. Benfatto, and L. Pietronero, Phys. Rev. Lett. **103**, 046404 (2009).

[38] Z. Yin, K. Haule, and G. Kotliar, Nature materials **10**, 932 (2011).

[39] J. Ferber, H. O. Jeschke, and R. Valentí, Physical Review Letters **109**, 236403 (2012).

[40] A. V. Chubukov, M. Khodas, and R. M. Fernandes, Phys. Rev. X **6**, 041045 (2016).

[41] K. Zantout, S. Backes, and R. Valentí, Physical Review Letters **123**, 256401 (2019).

[42] S. Bhattacharyya, K. Björnson, K. Zantout, D. Steffensen, L. Fanfarillo, A. Kreisel, R. Valentí, B. M. Andersen, and P. J. Hirschfeld, Phys. Rev. B **102**, 035109 (2020).

[43] V. Cvetkovic and O. Vafek, Phys. Rev. B **88**, 134510 (2013).

[44] F. Hund, Zeitschrift für Physik **99**, 119 (1936).

[45] J. O'Halloran, D. F. Agterberg, M. X. Chen, and M. Weinert, Phys. Rev. B **95**, 075104 (2017).

[46] M. H. Christensen, J. Kang, and R. M. Fernandes, Phys. Rev. B **100**, 014512 (2019).

[47] M. I. Aroyo, J. Perez-Mato, D. Orobengoa, E. Tasci, G. de la Flor, and A. Kirov, Bulg. Chem. Commun **43**, 183 (2011).

[48] Supplementary information. Includes further details on the numerical analysis and Refs. [9, 50, 51, 58–69].

[49] C. Fang, M. J. Gilbert, X. Dai, and B. A. Bernevig, Physical review letters **108**, 266802 (2012).

[50] K. Koepernik and H. Eschrig, Physical Review B **59**, 1743 (1999).

[51] J. P. Perdew and Y. Wang, Phys. Rev. B **45**, 13244 (1992).

[52] R. M. Dantas, F. Peña-Benitez, B. Roy, and P. Surówka, Physical Review Research **2**, 013007 (2020).

[53] N. Nagaosa, Journal of the Physical Society of Japan **75**, 042001 (2006).

[54] N. Nagaosa, J. Sinova, S. Onoda, A. H. MacDonald, and N. P. Ong, Reviews of modern physics **82**, 1539 (2010).

[55] D. Mou, T. Kong, W. R. Meier, F. Lochner, L.-L. Wang, Q. Lin, Y. Wu, S. L. Bud'ko, I. Eremin, D. D. Johnson, P. C. Canfield, and A. Kaminski, Phys. Rev. Lett. **117**, 277001 (2016).

[56] N. Hao and J. Hu, Phys. Rev. X **4**, 031053 (2014).

[57] E. Sheveleva, B. Xu, P. Marsik, F. Lyzwa, B. P. P. Mallett, K. Willa, C. Meingast, T. Wolf, T. Shevtsova, Y. G. Pashkevich, and C. Bernhard, Phys. Rev. B **101**, 224515 (2020).

[58] J. P. Perdew, K. Burke, and M. Ernzerhof, Phys. Rev. Lett. **77**, 3865 (1996).

[59] I. Opahle, K. Koepernik, and H. Eschrig, Physical Review B **60**, 14035 (1999).

[60] H. Eschrig, M. Richter, and I. Opahle, in *Theoretical and Computational Chemistry*, Vol. 14 (Elsevier, 2004) pp. 723–776.

[61] H. Eschrig, K. Koepernik, and I. Chaplygin, Journal of Solid State Chemistry **176**, 482 (2003).

[62] H. Eschrig, *The fundamentals of density functional theory*, Vol. 32 (Springer, 1996).

[63] K. Lejaeghere, G. Bihlmayer, T. Björkman, P. Blaha, S. Blügel, V. Blum, D. Caliste, I. E. Castelli, S. J. Clark, A. Dal Corso, *et al.*, Science **351** (2016).

[64] G. Kresse and J. Hafner, Phys. Rev. B **47**, 558 (1993).

[65] G. Kresse and J. Furthmüller, Computational materials science **6**, 15 (1996).

[66] G. Kresse and J. Furthmüller, Physical review B **54**, 11169 (1996).

[67] L. Elcoro, B. Bradlyn, Z. Wang, M. G. Vergniory, J. Cano, C. Felser, B. A. Bernevig, D. Orobengoa, G. Flor, and M. I. Aroyo, Journal of Applied Crystallography **50**, 1457 (2017).

[68] D. Mou, T. Kong, W. R. Meier, F. Lochner, L.-L. Wang, Q. Lin, Y. Wu, S. BudKo, I. Eremin, D. D. Johnson, *et al.*, Physical review letters **117**, 277001 (2016).

[69] G. H. Wannier, Phys. Rev. **52**, 191 (1937).